

# Shallow Water Three-Dimensional Transient Electromagnetic Modelling by Using Fictitious Wave Field Methods

Yanju Ji<sup>1,2</sup>, Xiangdong Meng<sup>1</sup>, and Guiying Ren<sup>1</sup>

<sup>1</sup> College of Instrumentation and Electrical Engineering  
Jilin University, Changchun, China  
{jiyj@jlu.edu.cn, 1581900057}@qq.com

<sup>2</sup> Key Laboratory of Geophysical Exploration Equipment  
Ministry of Education, Jilin University, Changchun, China  
261479384@qq.com

**Abstract** — The marine transient electromagnetic method is a valuable means for locating mineral resources because of its higher detection resolution as well as other advantages. However, this method is easily affected by the air layer and complex terrain, which significantly increase its calculation times. We addressed this problem by developing a three-dimensional finite-difference method based on the principle of correspondence between the diffusive and fictitious wave fields. Using a fast-iteration formula appropriate for a large time step, solving the Maxwell equations in a fictitious wave field, and the effects of air and seawater parameters on the electromagnetic response in shallow water are discussed. Choosing the first derivative of a Gaussian as a source, the 3D numerical simulation of transient electromagnetics in a shallow water area is realized. Comparing to the existing methods, the effectiveness of the proposed method is verified. The results show that this method enables fast and high-precision numerical calculations for 3D models and provides theoretical guidance for detecting seabed mineral resources in complex geological environments in shallow water.

**Index Terms** — Air layer, complex terrain, fictitious wave field, shallow water, three-dimensional modeling.

## I. INTRODUCTION

There are transitional zones between land and the sea. Such areas, also known as the coastal ocean, have a complex geological structure. Because the coastal marine shelf contains abundant hydrocarbon reservoirs and mineral resources, marine electromagnetic detection in shallow waters has become a research hotspot. The transient electromagnetic method has a higher resolution in shallow-sea high-resistance reservoirs compared to that of the frequency-domain electromagnetic method [1] because the latter is seriously affected by air wave

interference in shallow water, whereas the former can effectively separate the air waves and the response from the submarine formation [2]. Therefore, considerable attention has been paid to the use of the transient electromagnetic method in shallow waters [3]. However, the complex structure of the shallow continental shelf makes 3D numerical simulation extremely time-consuming, particularly if calculation of the air layer is included. This consideration is problematic because, when ocean exploration is carried out in areas with complex seabed topography, ignoring its effects may lead to misinterpretation of the seabed geological structure. Therefore, it is necessary to discover a means to carry out effective and rapid simulation that incorporates the air layer and complex terrain.

Analysis of a one-dimensional numerical simulation of a transient electromagnetic field in shallow water revealed that, when calculating a deep high-resistance model, the influence of the air layer can be neglected; however, when calculating a medium- or shallow-depth high-resistance body, the accuracy of the electromagnetic calculation will be impacted if the air layer is neglected in the calculations [4]. Applying both the time-domain finite-difference method and frequency-domain method to one-dimensional numerical simulation of shallow waters, it was found that the time-domain method can be effectively used to isolate the air layer, and it resolves seabed gas hydrate resources better than the frequency-domain method [5]. Mao et al. proposed a new absorbing boundary condition (ABC). When ABC is used in FDTD, it can effectively improve the computational efficiency [6]. Inoue and Asai proposed a new finite-difference time-domain (FDTD) based on hybrid implicit-explicit and multi-GPU techniques that can effectively improve the calculation efficiency [7]. Further, Ji et al. achieved good results when using the fictitious wave domain finite-difference method to simulate the three-dimensional

transient electromagnetism of land using a magnetic source [8].

The time-domain marine electromagnetic method is an effective means of shallow water resource detection. The distribution of seabed resources is uneven and spatially varies. One-dimensional and two-dimensional models cannot accurately simulate the real electromagnetic response from the subsurface. Moreover, achieving rapid iteration and efficient calculation for models incorporating the air layer and a complex seabed topography has become an urgent 3D computing problem. This study effectively resolves the inefficiency of three-dimensional electromagnetic numerical simulation for these cases and achieves numerical simulation of transient electromagnetism from a finite-length wire source in a shallow water region.

## II. TRANSFORMATION BETWEEN DIFFUSIVE AND FICTITIOUS WAVE FIELDS

When the time-domain finite-difference method is used to simulate the 3D electromagnetic field in shallow water, it is necessary to include the air layer for differential iteration. Because of the high resistivity of the air layer, the iterative calculation requires a large time step making it difficult for ordinary computers to complete the numerical calculations. We refer readers to read [8-9] for the details of its theory. This study expanded upon the basis of the research of [8]. The difference in [8] is that in document 8, the uniform grid is used to cut the three-dimensional model. It is assumed that the grid size in all calculation areas is equal. However, this will greatly reduce the computational efficiency. To improve the computational efficiency, in this study, the air layer is divided into a non-uniform grid, loading the CFS-PML boundary conditions in a fictitious wave field. In addition, the loop source is used in [8]. In this paper, a long wire source is selected, and the iterative relationship in the real diffusion field is transformed into the fictitious wave field for calculation. After the calculation is completed, the electromagnetic response in the fictitious wave field is transformed back to the real diffusion field. This process effectively solves the problem of an excessively long iteration time. The process of transformation proceeds as follows.

The first step is to transform the real diffusion field to a fictitious wave field. The frequency domain quasi-static Maxwell equation of the true diffusion field is as follows:

$$-\nabla \times H + \sigma E = -J, \quad (1)$$

$$\nabla \times E - i\omega\mu H = -K, \quad (2)$$

where  $\omega$  is the angular frequency in the real diffusion field;  $\varepsilon$  is the permittivity in the real diffusion field;  $\mu$  is the scalar-magnetic constant  $\mu = 4\pi \times 10^{-7}$ ;  $\sigma$  is the electric conductivity;  $J$  and  $K$  are the current density and

magnetic current density, respectively; and  $E$  and  $H$  are the electric and magnetic fields, respectively.

The angular frequencies in the real diffusion field and the fictitious wave field satisfy the following relationship:

$$-i\omega' = \sqrt{-2i\omega\omega_0}, \quad (3)$$

where  $\omega_0 = 2\pi \times f_0$  is the scaling parameter,  $f_0 = 1\text{Hz}$ , and  $\omega'$  is the conversion parameter between the fictitious wave field and real diffusion field.

To realize the transformation between the real and fictitious fields, we define a fictitious dielectric permittivity tensor from a conductivity tensor as follows:

$$\sigma = 2\omega_0\varepsilon'. \quad (4)$$

Formula (3) can be used to convert the electric and magnetic fields in the real domain into the fictitious wave domain. The frequency domain form is expressed as follows:

$$-\nabla \times H + 2\omega_0\varepsilon' E = -J', \quad (5)$$

$$\nabla \times E - i\omega'\mu H = -K'. \quad (6)$$

The Fourier transform is then applied to equations (5) and (6) to obtain the expression of the time-domain fictitious wave domain as follows:

$$-\nabla \times H' + \varepsilon' \partial_t E' = -J', \quad (7)$$

$$-\nabla \times E' + \mu' \partial_t H' = -K', \quad (8)$$

where  $J'$  and  $K'$  are the current density and magnetic current density in the fictitious wave domain, respectively, and  $E$  and  $H$  are the electric and magnetic fields in the fictitious wave domain.

The second step is the transformation from the fictitious wave field to the real diffusion field.

The purpose of transforming the real diffusion field into the fictitious wave field is to facilitate the calculation and improve the calculation efficiency. We can regard the real diffusion field as the real domain, the fictitious wave field as the fictitious domain, and the electromagnetic wave in the fictitious wave field as the fictitious wave. However, the fictitious wave field and fictitious wave itself have no physical significance; they have a hypothetical existence. Further, the calculated electromagnetic response in the fictitious wave field has no practical physical significance. Therefore, to obtain the real electromagnetic response, it is necessary to transform the calculation result of the fictitious wave field into the real diffusion field. The transformation relationship is as follows:

$$J(\omega) = \int_0^T J'(t') e^{-\sqrt{i\omega\omega_0}t'} e^{i\sqrt{i\omega\omega_0}t'} dt', \quad (9)$$

$$E(\omega) = \sqrt{\frac{-i\omega}{2\omega_0}} \int_0^T E'(t') e^{-\sqrt{i\omega\omega_0}t'} e^{i\sqrt{i\omega\omega_0}t'} dt', \quad (10)$$

$$H(\omega) = \int_0^T H'(t') e^{-\sqrt{i\omega\omega_0}t'} e^{i\sqrt{i\omega\omega_0}t'} dt', \quad (11)$$

$$K(\omega) = \sqrt{\frac{-i\omega}{2\omega_0}} \int_0^T K'(t') e^{-\sqrt{i\omega\omega_0}t'} e^{i\sqrt{i\omega\omega_0}t'} dt', \quad (12)$$

where  $T$  is the total calculation time in the fictitious wave field and  $t'$  is the sampling time.

### III. SHALLOW WATER FICTITIOUS TIME-DOMAIN FINITE-DIFFERENCE METHOD

#### A. Difference equation in the fictitious wave field

When the finite-difference method is applied to solve the governing equation of the time domain in the fictitious wave field, a non-uniform mesh is used. Smaller meshing is used at the centre of the calculation, and a larger grid calculation is used at more distant locations. The finite-difference forms of the magnetic field and electric field are as follows:

$$E_{x_i+1/2,j,k}^{n+1} = E_{x_i+1/2,j,k}^n + \Delta t \frac{2\omega_0}{\sigma} (\partial_y^- H_{z_i+1/2,j,k+1/2}^{n+1/2} - \partial_z^- H_{y_i+1/2,j,k+1/2}^{n+1/2}) - \Delta t \frac{2\omega_0}{\sigma} J_x, \quad (13)$$

$$E_{y_i,j+1/2,k}^{n+1} = E_{y_i,j+1/2,k}^n + \Delta t \frac{2\omega_0}{\sigma} (\partial_z^- H_{x_i,j+1/2,k+1/2}^{n+1/2} - \partial_x^- H_{z_i+1/2,j+1/2,k}^{n+1/2}) - \Delta t \frac{2\omega_0}{\sigma} J_y, \quad (14)$$

$$E_{z_i,j,k+1/2}^{n+1} = E_{z_i,j,k+1/2}^n + \Delta t \frac{2\omega_0}{\sigma} (\partial_x^- H_{y_i+1/2,j,k+1/2}^{n+1/2} - \partial_y^- H_{x_i,j+1/2,k+1/2}^{n+1/2}), \quad (15)$$

$$H_{x_i,j+1/2,k+1/2}^{n+1/2} = H_{x_i,j+1/2,k+1/2}^{n-1/2} - \frac{\Delta t}{\mu} (\partial_y^+ E_{z_i,j,k+1/2}^n - \partial_z^+ E_{y_i,j+1/2,k}^n), \quad (16)$$

$$H_{y_i+1/2,j,k+1/2}^{n+1/2} = H_{y_i+1/2,j,k+1/2}^{n-1/2} - \frac{\Delta t}{\mu} (\partial_z^+ E_{x_i+1/2,j,k}^n - \partial_x^+ E_{z_i,j,k+1/2}^n), \quad (17)$$

$$H_{z_i+1/2,j+1/2,k}^{n+1/2} = H_{z_i+1/2,j+1/2,k}^{n-1/2} - \frac{\Delta t}{\mu} (\partial_x^+ E_{y_i,j+1/2,k}^n - \partial_y^+ E_{x_i+1/2,j,k}^n), \quad (18)$$

where  $e_x(i, j, k)$ ,  $e_y(i, j, k)$ , and  $e_z(i, j, k)$  are the electric fields in the three directions,  $x$ ,  $y$ , and  $z$ , in the fictitious wave field, respectively;  $h_x(i, j, k)$ ,  $h_y(i, j, k)$ , and  $h_z(i, j, k)$  are the magnetic fields in the  $x$ ,  $y$ , and  $z$  directions in the fictitious wave field; and  $\Delta t'$  is the time step in the fictitious wave field.  $\partial_{x,y,z}^+$  is the forward derivative operator,  $\partial_{x,y,z}^-$  is the backward derivative operator.

During the process of solving the equations, we need to pay attention to  $\sigma$ , which is the average conductivity of adjacent grids. In this paper, the current source is used to simulate the emission source of the time-domain electromagnetic method; therefore, the magnetic current source can be set to zero.

#### B. Fast iterative time step method

When using variable time steps for the 3D electromagnetic numerical calculation for shallow water, as time increases, the step size increases, resulting in a long calculation time that is not conducive to efficiency. Therefore, in the fictitious wave field, the variable time step expression is re-determined incorporating the electromagnetic response speed in seawater as follows:

$$\Delta t' = \frac{\Delta x}{\sqrt{3}C_{\max}}. \quad (19)$$

We assume the resistivity isotropic is equal to  $\rho(x)$ , where  $C(x)_{\max} = \sqrt{\frac{2\omega_0\rho(x)_{\max}}{\mu}}$  is the maximum propagation velocity of the signal in seawater and  $\Delta x$  is

the minimum spacing length in the mesh. The maximum time required for the signal to reach the  $R_{\max}$  (offset distance) in the fictitious wave field is as follows:

$$T_{\max} = \frac{R_{\max}}{C_{\min}}, \quad (20)$$

where  $R_{\max}$  and  $C_{\min}$  are the maximum distance between the transmission and reception and the minimum electromagnetic wave propagation speed, respectively.

The number of iteration steps in the fictitious wave field is expressed as follows:

$$N_t = \frac{T_{\max}}{\Delta t} = \frac{\sqrt{3}R_{\max}}{\Delta x} \times \sqrt{\frac{\rho_{\max}}{\rho_{\min}}}, \quad (21)$$

where  $\rho_{\max}$  and  $\rho_{\min}$  are the maximum resistivity and minimum resistivity, respectively;  $\Delta x$  is the minimum spacing length in the grid; and  $R_{\max}$  is the maximum distance between transmission and reception.

The computational efficiency of the time step in the diffusive and fictitious wave fields can be compared by using the time step calculation formula in the diffusive field as follows:

$$\Delta t = \alpha \sqrt{\frac{\mu\sigma^{\min}}{6}} \Delta x, \quad (22)$$

where  $\alpha$  is 0.1–0.2,  $\sigma^{\min}$  is the minimum conductivity, and  $t$  is the length of time determined according to the selected initial moment. We use an evenly spaced half-space model for testing. The grid size is set to 100 m; the conductivity is 10, 50, and 100 S/m; and the transceiver distance is 10,000 m. The computer used for this test is configured with an i7-7700 CPU and 32.0 GB of RAM. The iteration time step and number of iterations are listed in Table 1.

Table 1: Comparison of computational efficiency between the fictitious wave domain FDTD (finite difference time domain) and traditional FDTD

	FDTD		FWD-FDTD	
	Iteration Steps	Calculation Time	Iteration Steps	Calculation Time
$\sigma = 10\text{S/m}$	2933	1552 s	302	160 s
$\sigma = 50\text{S/m}$	6556	3269 s	675	346 s
$\sigma = 100\text{S/m}$	9266	4246 s	954	447 s

Comparison of the computational efficiency of the fictitious wave domain finite-difference time domain (FWD-FDTD) and the traditional FDTD indicates that the FDTD iteration step is positively correlated with conductivity: as conductivity increases, the number of iteration steps gradually increases. However, in the fictitious wave field, the increase in the number of iteration steps is smaller than that in the diffusive field. The number of iterations is reduced by more than 9 times in the fictitious wave field because the ratio of

the maximum and minimum conductivity determines the speed of the iterative calculation in the fictitious domain; in the diffusive domain, the number of iteration steps depends only on the minimum conductivity, and the calculation time depends on the change in conductivity. As the conductivity increases, the calculation time also increases; however, in the fictitious domain, the time is increased by more than 9 times, and a fast calculation is realized.

#### IV. PARAMETRIC ANALYSIS FOR SEAWATER AND AIR LAYERS IN SHALLOW WATER

##### A. Influence of the seawater layer thickness

In this section, we use a three-layer model comprising air, seawater, and seabed to analyse the influence of seawater depth on the electric field. The air conductivity is 10-10 S/m, the seawater conductivity is 3.3 S/m, and the submarine conductivity is 0.1 S/m. Values of 0, 200, 400, and 1200 m are used for the seawater thickness. The electric field response curve is shown in Fig. 1.

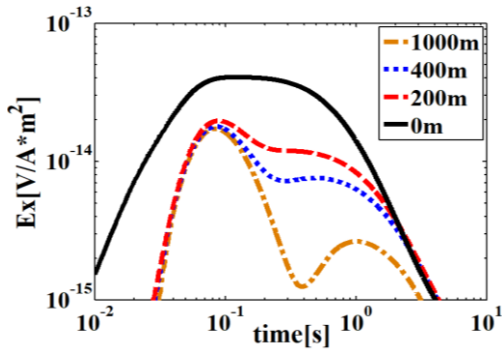


Fig. 1. Influence of seawater thickness.

The black, red, blue, and yellow response curves in Fig. 1 represent seawater thicknesses of 0, 200, 400, and 1200 m, respectively. The figure shows that as the thickness of the seawater decreases, the air wave interference becomes more pronounced, and the response attributable to the direct wave decreases. When the thickness of the seawater approaches zero, only the air wave exists during the early stages. Thus, in shallow water areas, the peak of the direct wave is not obvious due to interference from air waves. It can be concluded that the response of the air and the seawater cannot be considered negligible in shallow water areas. During the actual detection process, the presence of air waves is real and inevitable. When the FWD-FDTD method is used to simulate the air wave, its influence is mainly concentrated during the early stages, while the influence of the high-resistance and low-resistance anomalies is mainly concentrated during the late stages. Therefore, the influence of the air can be eliminated by choosing an appropriate time point.

##### B. Optimization of the air layer model

In the diffusion field, the number of iteration steps is proportional to the minimum conductivity; air has a low conductivity. If the air is directly divided, it will lead to a large increase in the number of iteration steps. The calculation of the air layer is typically avoided by means of upward continuation, but the accuracy of the early calculations is significantly reduced. In the fictitious wave field, the number of iteration steps depends on the ratio of the maximum and minimum conductivity and does not depend on a fixed number. Thus, the high-resistance air layer can be directly divided and calculated. In this study, the air layer is divided into a non-uniform grid with the Cartesian coordinate system, as shown in Fig. 2. During the modelling process, we need to pay attention to the selection of the air layer conductivity. The real air layer conductivity tends to be infinitesimal. If the conductivity is too large, it will not represent the actual situation. If the conductivity is too small, it will increase the calculation efficiency. Considering the calculation efficiency of the fictitious wave field, the air layer conductivity in this paper is  $10^{-10}$  S/m.

The z axis is positive, assuming that the conductivity and permeability are constant within each prism. The Courant-Friedrichs-Lewy (CFL) limitation is employed as the stability condition in the fictitious wave domain as follows:

$$\Delta t \leq \frac{1}{c_{\max} \sqrt{\frac{1}{\Delta x^2} + \frac{1}{\Delta y^2} + \frac{1}{\Delta z^2}}}$$

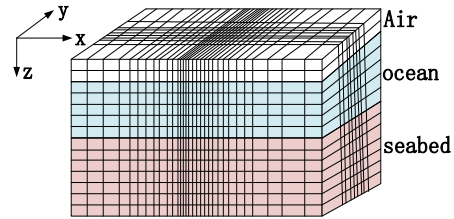


Fig. 2. Air layer grid diagram.

#### V. LIMITED LENGTH WIRE SOURCE LOADING IN SHALLOW WATER TRANSIENT ELECTROMAGNETIC MEASUREMENT

##### A. Pulse emission excitation source loading

In shallow water, the source is near the sea-air interface and will be disturbed by air; thus, the initial time will be difficult to determine. Thus, loading the initial field is no longer applicable. Furthermore, in reality, the excitation source of a marine electromagnetic measurement system is a pulse or trapezoidal wave, not a step wave. To solve the problem of complex excitation source loading, we directly load the source in the fictitious wave field. This loading process can be decomposed into two steps.

First, it is necessary to select the basic emission current signal of the excitation source according to the point source Green function expression,  $G_E(\omega) = \frac{E_r(\omega)}{J_s(\omega)}$ .

An important principle to be followed is that the zero-frequency component of the emission current signal is not zero. The second step is to convert the fictitious into the actual emission current signal. The fictitious emission source is different from the actual; it does not have any real meaning. There is a proportional integral relationship between the two that can be used to convert between the fictitious and actual emission sources.

When using the transient electromagnetic method for shallow water, a pulse source provides a higher resolution than that of a step source [10]. The first derivative of a Gaussian source is thus selected as follows:

$$T_{\max} = \frac{R_{\max}}{C_{\min}}, \quad (23)$$

where  $f_{\max}^2$  is the maximum frequency of the electromagnetic field transmission in the fictitious wave field and  $\beta = \pi f_{\max}^2 t_0 = \pi / f_{\max}$ .

We choose the first derivative of a Gaussian as a fictitious source. It is dimensionless and not real, as follows:

$$J_n(\omega) = 2\omega_0 e^{-\frac{i\omega a_0}{2\beta_0}} e^{-\sqrt{\omega a_0 t_0}} e^{\sqrt{\omega a_0 t_0}}. \quad (24)$$

If  $\omega = 0$ , formula (24) provides the current density as  $J_n(\omega) = 2\omega_0$ ; thus, the principle that the zero-frequency component is not zero is satisfied. The loading mode and emission signal waveform in the fictitious wave field are shown in Figs. 3 and 4. When loading the emission current signal, it is necessary to ensure that the fictitious emission current has an independent direction. The fictitious emission source current is consistent with the direction and density distribution of the real current. In this paper, the electric source excitation ensures that the z-direction electric field component of the fictitious source is zero.

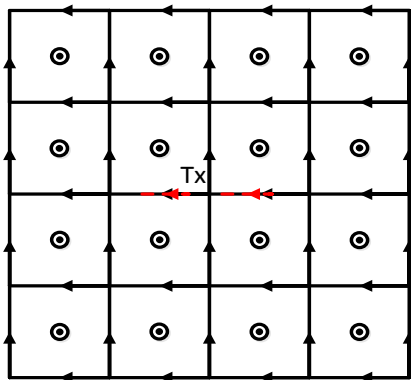


Fig. 3. Long wire source loading method.

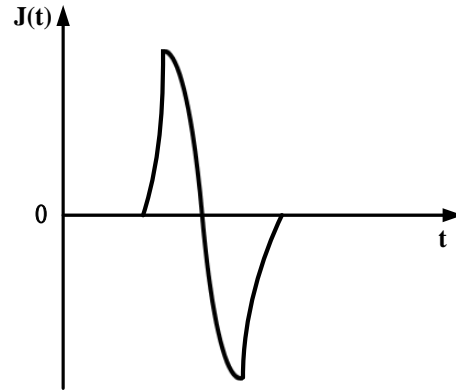


Fig. 4. Source waveform.

### B. Analysis of the influence of the launch source wire length

In marine numerical simulations, the source is often approximated to an electric dipole [11], ignoring the source length. Because of geographical terrain and other constraints, the observation point and the emission source in actual ocean exploration often do not meet the appropriate conditions to assume this. Therefore, the electromagnetic response of a finite-length source needs to be calculated. This study examines the influence of the field source length by calculating the electric field response under different wire length excitations. The three-dimensional model is shown in Fig. 5. The air layer has a conductivity of  $10^{-10}$  S/m, and the seawater layer has a conductivity of 3.3 S/m and a thickness of 200 m. The conductivity of the sea bottom layer is 0.1 S/m. A high-resistance body with a conductivity of 0.01 S/m is placed at a distance of 100 m from the seabed. The electromagnetic response is then calculated for a 200-, 400-, and 1000-m-long wire source. The resulting electric field response curves are shown in Fig. 6.

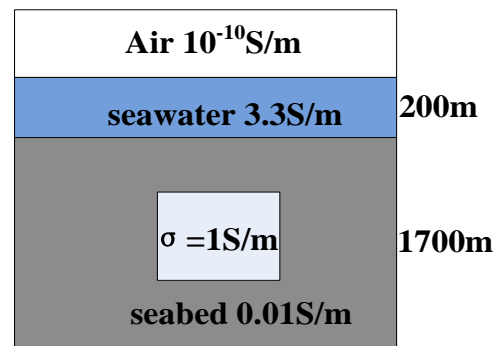


Fig. 5. Three-dimensional high-resistance model.

With an increase in the wire source length, the amplitude of the response also increases. There is a significant change in the response of the anomaly during the late stages. When the distance between the

transmission and reception is 2000 m, a wire source 200 and 400 m in length can be approximated as a point source; however, during the actual detection process, the basic characteristics of a point source cannot be satisfied in many cases. Thus, the length of the source needs to be fully considered in the three-dimensional numerical simulation.

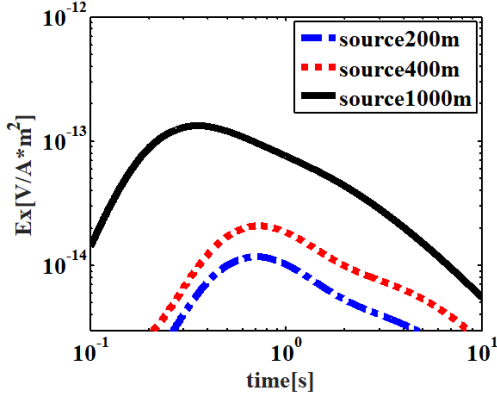


Fig. 6. Electric field response curves for different wire lengths.

### C. Loading the CFS-PML boundary conditions in the fictitious wave field

The perfectly matched layer (PML) has been able to absorb the electromagnetic wave in the FDTD [12]. Roden proposes a convolutional PML (CFS-PML) based on PML and recursive convolution [13].

CFS-PML is widely used because of its good absorption effect and savings in computational memory. Hu applied CFS-PML to the solution of a wave equation in a fictitious wave domain, which improved the absorbing effect of the boundary on evanescent and low frequency waves [14]. To improve the calculation efficiency, this paper uses CFS-PML as a boundary condition to absorb the electromagnetic wave.

Taking the X direction as an example, in this coordinate space, we use Maxwell's curl equations as follows:

$$\nabla_s \times H'(\omega') + i\omega' \varepsilon' E'(\omega') = 0, \quad (25)$$

$$\nabla_s = \frac{1}{\hat{s}_x} \frac{\partial}{\partial x} \mathbf{i} + \frac{1}{\hat{s}_y} \frac{\partial}{\partial y} \mathbf{j} + \frac{1}{\hat{s}_z} \frac{\partial}{\partial z} \mathbf{k}, \quad (26)$$

where  $\hat{s}_x$ ,  $\hat{s}_y$ ,  $\hat{s}_z$  is the nondimensional stretching variable,  $\hat{s}_i = k_i + \frac{\sigma_i}{\alpha_i + i\omega\varepsilon'}$  ( $i = x, y, z$ );  $\sigma_i$  ( $i = x, y, z$ ) is the conductivity of the CFS-PML layers; and  $k_i$  and  $\alpha_i$  are the positive real numbers  $\alpha_i > 0$ ,  $\sigma_i > 0$ , and  $k_i \geq 1$ . When the  $k_i = 1$  and  $\alpha_i = 0$ , it will degenerate into the original PML boundary condition.

Taking the  $E'_x$  direction as an example, from

equations (25) and (26), we can obtain the following:

$$i\omega' \varepsilon' E'_x(\omega') = -\left( \frac{1}{\hat{s}_y} \frac{\partial H'_z(\omega')}{\partial y} - \frac{1}{\hat{s}_z} \frac{\partial H'_y(\omega')}{\partial z} \right). \quad (27)$$

Using Laplace transform, from formula (29), the iterative expression of  $E'_x$  can be obtained as follows:

$$E'_{x_{i+1/2,j,k}}{}^{n+1} = E'_{x_{i+1/2,j,k}}{}^n + \Delta t \frac{2\omega_0}{\sigma} [\partial_y^{-1} H'_{z_{i+1/2,j+1/2,k}}{}^{n+1/2} - \partial_z^{-1} H'_{y_{i+1/2,j,k+1/2}}{}^{n+1/2}] + \Delta t \frac{2\omega_0}{\sigma} (\Psi_{e_{y_{i+1/2,j,k}}}{}^{n+1/2} - \Psi_{e_{z_{i+1/2,j,k}}}{}^{n+1/2}), \quad (28)$$

$$\Psi_{e_{y_{i+1/2,j,k}}}{}^{n+1/2} = b_y \Psi_{e_{y_{i+1/2,j,k}}}{}^{n-1/2} + a_y (H'_{z_{i+1/2,j+1/2,k}}{}^{n+1/2} - H'_{z_{i+1/2,j-1/2,k}}{}^{n+1/2}) / \Delta_y, \quad (29)$$

$$\Psi_{e_{z_{i+1/2,j,k}}}{}^{n+1/2} = b_z \Psi_{e_{z_{i+1/2,j,k}}}{}^{n-1/2} + a_z (H'_{y_{i+1/2,j+1/2,k}}{}^{n+1/2} - H'_{y_{i+1/2,j-1/2,k}}{}^{n+1/2}) / \Delta_z. \quad (30)$$

## VI. NUMERICAL CALCULATION OF THE ELECTROMAGNETIC RESPONSE OF A COMPLEX MODEL IN SHALLOW WATER

### A. Algorithm verification

We verify the algorithm by considering a classic layered model with a seawater depth of 300 m and resistivity  $\rho = 0.3 \Omega \cdot m$ , as shown in Fig. 7. Two values are used for the distance between the receiver and transmitter: 1000 and 1100 m. The calculated results are compared to those of [7] as shown in Fig. 8. The calculation results plotted in Fig. 8 indicate that the electromagnetic response curve is consistent at the different offsets.

To further validate the algorithm, we evaluate its validity for complex three-dimensional geological conditions by using the three-dimensional complex geological models presented by [6] for comparative analysis. The model settings are shown in Fig. 9. The air conductivity is  $10^{-10} \text{ S/m}$ , and the background conductivity is  $0.02 \text{ S/m}$ . There is a mountain and valley to the left and right of the transmitting source, Tx is the transmitting source position, and Rx is the receiving source position. The electric field response is shown in Fig. 9, and the relative error is shown in Fig. 10.

$\rho = 0.3 \Omega \cdot m$
$\rho = 0.5 \Omega \cdot m$
$\rho = 1.5 \Omega \cdot m$
$\rho = 100 \Omega \cdot m$
$\rho = 2 \Omega \cdot m$

Fig. 7. Shallow water high-resistivity layered model.

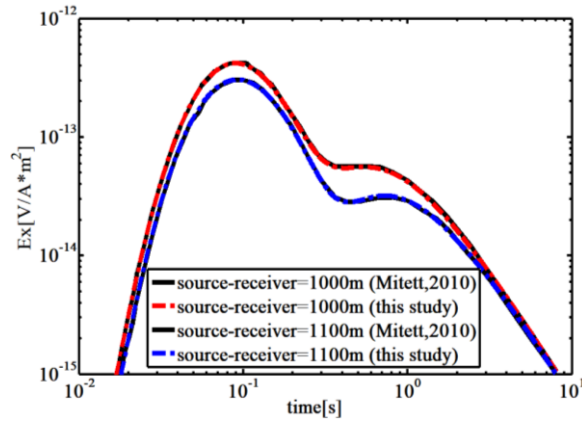


Fig. 8. Response curve of the layered model.

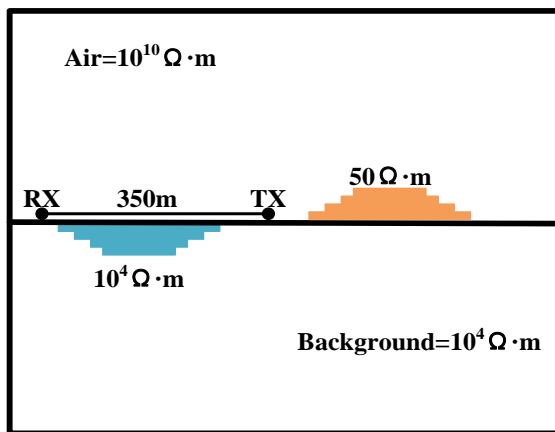


Fig. 9. 3D complex geological model.

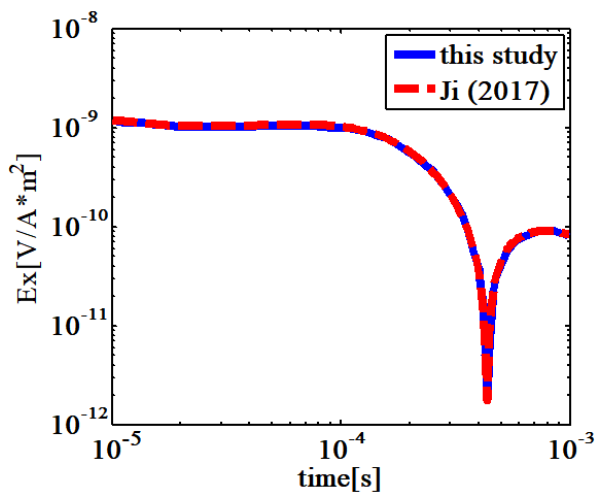


Fig. 10. Comparison of the electric field response at the  $R_{X1}$  receiving position.

Figure 10 shows that the response curve and results of [6] are basically consistent for undulating terrain,

which supports the validity of the present method for such terrain.

### B. Multi-object model in shallow water

The 3D transient electromagnetic response of shallow anomalies was analysed by designing a layered earth model with 3D anomalous bodies as shown in Fig. 11. The grid dimensions are  $100 \times 100 \times 70$ , the air layer thickness is 2000 m, the air conductivity is  $10^{-10}$  S/m, the seawater layer thickness is 100 m, the low-resistance layer beneath the sea is 300 m thick, the conductivity of the low-resistance layer is 1 S/m, and the conductivity of the seabed layer is 0.1 S/m. There are three abnormal bodies that have an electrical conductivity of 30 S/m. The electric field response is shown in Fig. 12. Figures 13 (a) and (b) show profile views of the induced current in the fictitious wave field.

Figure 13 clearly shows the positions of the high-resistance layer and anomalous bodies. Under the influence of the high-resistance layer, the propagation direction of the electromagnetic wave no longer symmetrically propagates. The overall trend of the curve is similar to that of the layered model. For the responses of the air and sea layers, the response of the anomalous body occurs during a late stage.

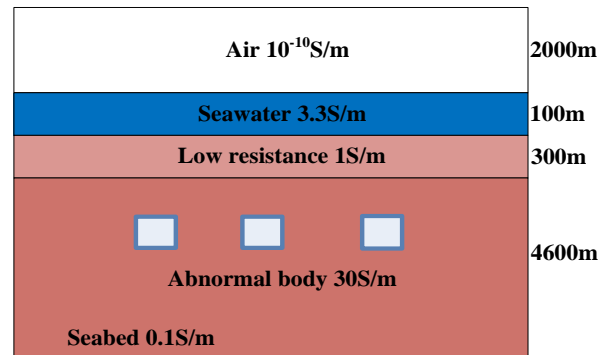


Fig. 11. 3D low-resistance complex model.

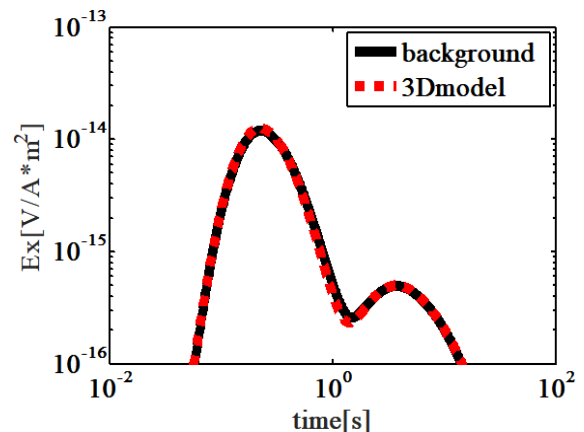


Fig. 12. Response curve of the three-dimensional model.

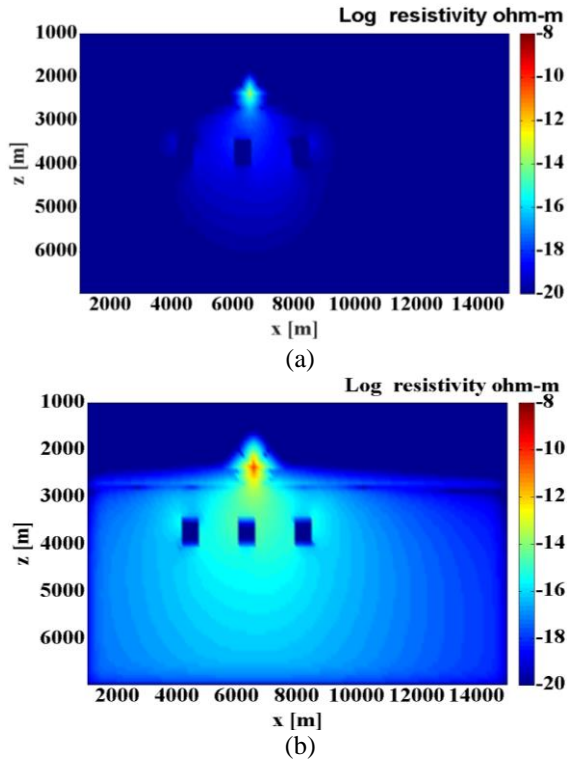


Fig. 13. Snapshots of the induced current system in the fictitious wave field (y direction 2000 m).

**C. High-resistance model of complex terrain in shallow water**

Complex terrain environments were simulated by designing a 3D model, as shown in Fig. 14. Tx represents the source location, which is 200 m in length. Rx represents the receiving point. The transmission and reception distance is 600 m, the seawater layer resistivity is  $0.3 \Omega \cdot m$ , and the sea bottom resistivity is  $0.5 \Omega \cdot m$ . There is convex and concave topography on the left and right sides of the emission source, the seawater layer is 200 m in thickness, and the thickness of the rock layer beneath the sea is 800 m.

The results for the calculated response are shown in Fig. 15. The response of a high-resistance anomaly under the undulating terrain is blue, whereas that of pure undulating terrain is red. To better analyse the influence of the undulating terrain, Figs. 16 (a) and (b) show snapshots of the induced current system in the fictitious wave field at different times.

The seabed topography can be clearly seen in Fig. 16. The peaks and valleys are, respectively, located on the left and right sides of the transmission source, and there is a high-resistance anomaly on the seabed. Because of the influence of the topography, the response curve has significantly changed, and the electric field response can be seen during the early and late stages, confirming the necessity of simulating the terrain. In

the fictitious wave field, the change in the transmission source is clearer than that in the diffusion field. Therefore, the generated induced current will more violently fluctuate. The means by which the electromagnetic field is transmitted is changed by undulating the submarine terrain such that it no longer symmetrically spreads. The influence of undulating terrain on the response curve is mainly concentrated during the early stages, whereas the response of the three-dimensional anomaly on the seabed is mainly concentrated during the late stages. Therefore, undulating terrain cannot be ignored in a shallow-sea ocean transient electromagnetic simulation.

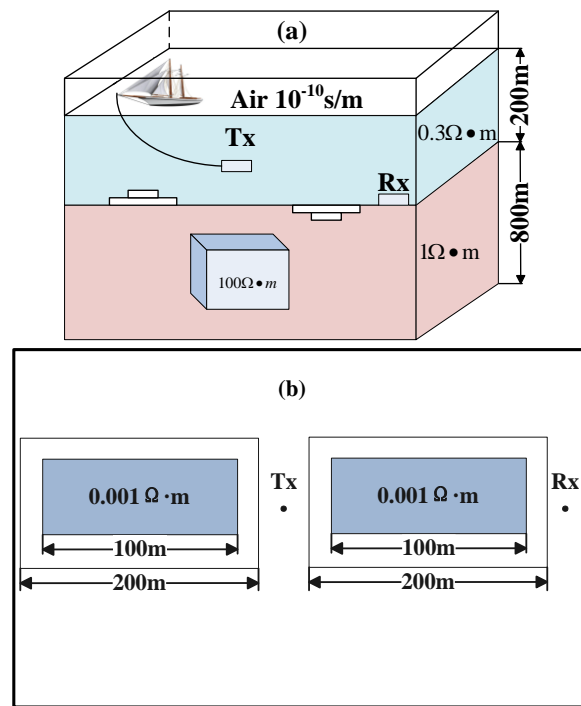


Fig. 14. Schematic diagram of undulating terrain: (a) front view and (b) top view.

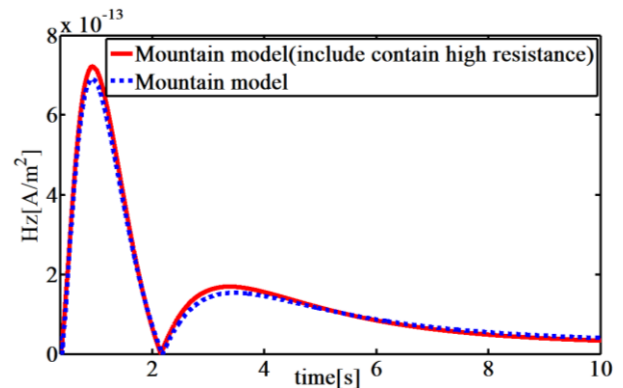


Fig. 15. Electromagnetic response for complex seabed geomorphology, including a high-resistance anomaly.

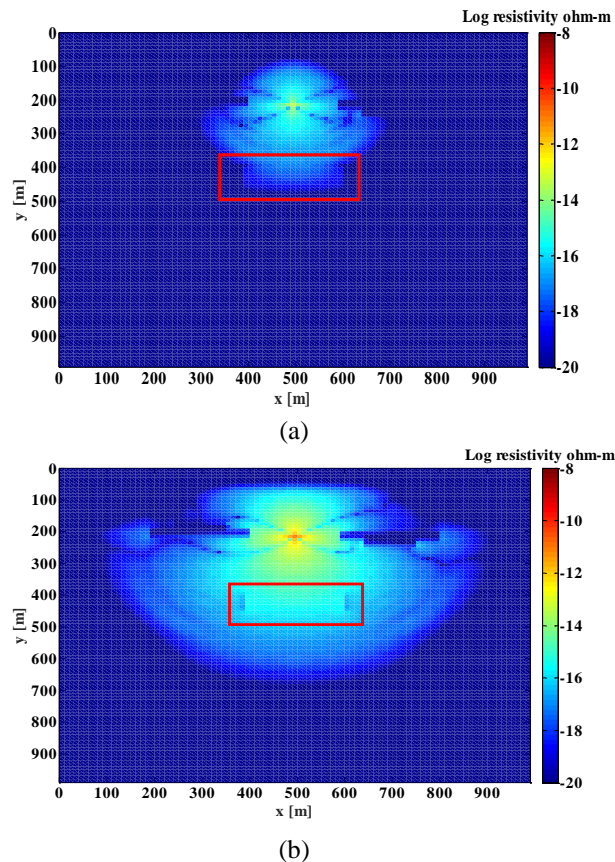


Fig. 16 Snapshots of the induced current system of undulating terrain in the fictitious wave field ( $y$  direction 2000 m).

## V. CONCLUSION

We propose a new, fast method for shallow water three-dimensional electromagnetic forward modelling. The method is based on the correspondence between the diffusive and fictitious wave fields and can be applied to the forward calculation of undulating terrain in shallow water. The efficiency of electromagnetic numerical calculation is improved by defining the iteration time step size formula in the fictitious wave field. When the depth of the seawater layer or the anomalous body is shallow, there is a non-negligible response from the air and seawater layers. Using a pulse source signal in the governing equation allows direct calculations incorporating the source to be realized, in turn enabling three-dimensional electromagnetic numerical simulation of complex terrain. The complexity of the seabed topography affects the normal propagation of the electromagnetic wave, which greatly influences the resolution of shallow abnormal bodies. Forward simulation is the basis of data interpretation and imaging. In this paper, a shallow water 3D numerical simulation is realized, including the air layer and undulating terrain, which makes the simulation results more closely match

the real geological conditions. It can not only provide a basis for the exploration of underwater resources but also theoretical guidance for detection instrument design.

Given the scarcity of terrestrial resources, countries around the world have increased their demand for offshore seabed and deep seabed energy. The marine transient electromagnetic method can play an important role in marine resource detection. Although this paper realizes three-dimensional forward modelling of shallow waters, the distribution of geological structures and resources in the seabed is extremely complicated; their detection is made more challenging because of the polarization of seawater in ocean electromagnetic detection. Therefore, further research is necessary to study the electromagnetic and polarization responses in complex geological models.

## ACKNOWLEDGMENT

We thank editor and an anonymous reviewer for constructive suggestions. This work was supported by the National Natural Science Foundation of China (Grant Number 3A416AQ50537).

## REFERENCES

- [1] K. M. Strack, T. Hanstein, C. H. Stoyer, et al., "Time domain controlled source electromagnetics for hydrocarbon applications," 2011.
- [2] C. J. Weiss, "The fallacy of the "shallow-water problem" in marine CSEM exploration," [J]. *Geophysics*, vol. 72, no. 6, pp. A93-A97, 2007.
- [3] P. O. Barsukov and E. B. Fainberg, "Transient marine electromagnetics in shallow water: A sensitivity and resolution study of the vertical electric field at short ranges," *Geophysics*, vol. 79, no. 1, pp. E39-E49, 2014.
- [4] Y. G. Li and S. Constable, "Transient electromagnetic in shallow water: Insights from 1D modeling," *Chinese Journal of Geophysics*, vol. 53, no. 3, pp. 737-742, 2010.
- [5] D. Connell and K. Key, "A numerical comparison of time and frequency-domain marine electromagnetic methods for hydrocarbon exploration in shallow water," *Geophysical Prospecting*, vol. 61, no. 1, pp. 187-199, 2013.
- [6] Y. Mao, A. Z. Elsherbeni, S. Li, and T. Jiang, "Non-uniform surface impedance absorbing boundary condition for FDTD method," *Applied Computational Electromagnetics Society Journal*, vol. 33, no. 2, pp. 232-235, 2018.
- [7] Y. Inoue and H. Asai, "Efficient electromagnetic simulation including thin structures by using multi-GPU HIE-FDTD method," *Applied Computational Electromagnetics Society Journal*, vol. 33, no. 2, pp. 212-215, 2018.
- [8] Y. Ji, Y. Hu, and N. Imamura, "Three-dimensional transient electromagnetic modeling based on

fictitious wave domain methods,” *Pure & Applied Geophysics*, vol. 174, no. 5, pp. 2077-2088, 2017.

- [9] R. Mittet, “High-order finite-difference simulations of marine CSEM surveys using a correspondence principle for wave and diffusion fields,” *Geophysics*, vol. 75, no. 1, pp. F33-F50, 2010.
- [10] A. Avdeeva, M. Commer, and G. A. Newman, “Hydrocarbon reservoir detectability study for marine CSEM methods: Time-domain versus frequency-domain,” *Seg. Technical Program Expanded Abstracts*, vol. 26, no. 1, p. 3124, 2007.
- [11] S. Constable, “Review paper: Instrumentation for marine magnetotelluric and controlled source electromagnetic sounding,” [J]. *Geophysical Prospecting*, vol. 61, pp. 505-532, 2013.
- [12] J. P. Berenger, “A perfectly matched layer for the absorption of electromagnetic waves,” [M]. *Academic Press Professional, Inc.*, 1994.
- [13] J. A. Roden and S. D. Gedney. “Convolution PML (CPML): An efficient FDTD implementation of the CFS-PML for arbitrary media,” *Microwave and Optical Technology Letters*, vol. 27, no. 5, 2000.
- [14] Y. Hu, G. Egbert, Y. Ji, et al., “A novel CFS-PML boundary condition for transient electromagnetic simulation using a fictitious wave domain method,” *Radio Science*, vol. 52, no. 1, pp. 118-131, 2017.



**Yanju Ji** in 1997, graduated from Changchun University and received a master's degree. Graduated from Jilin University in 2004, majoring in Earth Exploration and Information Technology and received a doctorate degree. The main research direction is time domain electromagnetic theory and detection technology.



**Xiangdong Meng** graduated from Jilin University of Architecture in 2015, majoring in Industrial Design Engineering and received a Master's degree. In 2016, studying in Jilin University for a Ph.D. The main research area is three-dimensional numerical simulation of transient electromagnetic in time domain.



**Guiying Ren** graduated from Jilin University in 2017 and received a bachelor's degree. In 2017, studying in Jilin University for a master's degree. The main research area is three-dimensional numerical simulation of transient electromagnetic in time domain.